Absolute partial cross sections for electron-impact ionization of H_2, N_2, and O_2 from threshold to 1000 eV

H. C. Straub, P. Renault, B. G. Lindsay, K. A. Smith, and R. F. Stebbings
Department of Physics, Department of Space Physics and Astronomy, and Rice Quantum Institute, Rice University, Post Office Box 1892, Houston, Texas 77251
(Received 27 December 1995)

Absolute partial cross sections from threshold to 1000 eV are reported for electron-impact ionization of H_2, N_2, and O_2. Data are presented for the production of H_2^+ and H^+ from H_2; the production of N_2^+, $N^+ + N_2^{2+}$, and N^{2+} from N_2; and the production of O_2^+, $O^+ + O_2^{2+}$, and O^{2+} from O_2. The product ions are mass analyzed with a time-of-flight mass spectrometer and detected with a position-sensitive detector whose output provides clear evidence that all energetic fragment ions are collected. The overall uncertainty in the absolute cross-section values for singly charged parent ions is $\pm 3.5\%$ and is marginally higher for fragment ions. Previous cross-section measurements are compared to the present results. [S1050-2947(96)06709-1]

PACS number(s): 34.80.Gs

I. INTRODUCTION

Ionization of atoms and molecules by electron impact is of fundamental importance in atmospheric science, plasma processes, and mass spectrometry. An extensive review of the literature reveals, however, that although there have been many studies of the rare gases, few measurements have been reported for electron-impact ionization of molecules. Of these the most widely known and referenced are the absolute total cross-section measurements of Rapp and Englander-Golden [1]. Several experimenters have since employed mass spectrometry to measure partial cross sections for individual ionic products; however, almost without exception, these studies yielded relative cross sections that were then normalized to the absolute total cross sections, most commonly those measured by Rapp and Englander-Golden. The only truly absolute partial cross sections that have been previously reported for molecules appear to be those by Peterson [2] and Freund, Wetzel, and Shul [3] who used the fast neutral beam technique.

This paper reports absolute partial cross sections for electron-impact ionization of H_2, N_2, and O_2 from threshold to 1000 eV. The measured processes are the production of H_2^+ and H^+ from H_2, the production of N_2^+, $N^+ + N_2^{2+}$, and N^{2+} from N_2, and the production of O_2^+, $O^+ + O_2^{2+}$, and O^{2+} from O_2. The results are obtained with a time-of-flight mass spectrometer coupled with position-sensitive detection of the product ions. The individual cross sections for N^+ and N_2^{2+} and for O^+ and O_2^{2+} cannot be separately determined because each set of ions has the same mass-to-charge ratio and, therefore, the same flight times in the mass spectrometer.

II. APPARATUS AND EXPERIMENTAL METHOD

The apparatus shown in Fig. 1 has been previously discussed in detail [4]. Briefly, during a cross-section measurement the entire vacuum chamber is filled with the target gas at a pressure of approximately 3×10^{-6} Torr. At a repetition rate of 2.5 kHz, 20-ns-long pulses of approximately 2500 electrons are directed through an interaction region, located between two plates maintained at ground potential, and are then collected in a Faraday cup. Approximately 200 ns after each electron pulse, an electric field is applied across the interaction region to drive any positive ions formed by electron impact toward the bottom plate. This electric field is generated by applying a 2-kV pulse with a 300-ns rise time to the top plate. Some ions pass through a grid-covered aperture, of length 1.91 cm in the direction parallel to the electron beam, in the bottom plate. These ions are then accelerated, to an energy of 4.6 keV for singly charged ions, and subsequently impact a position-sensitive detector (PSD) that records both their arrival times and positions. This system is a time-of-flight mass spectrometer. The ion arrival times identify their mass-to-charge ratios and the ion arrival positions serve to demonstrate complete collection of energetic fragment ions from dissociative ionization.

Under conditions in which very few of the incident electrons produce an ion, the partial cross section $\sigma(X)$ for production of ion species X is given by

$$\sigma(X) = \frac{N_i(X)}{N_e n l}, \tag{1}$$

where $N_i(X)$ is the number of X ions produced by a number N_e of electrons passing a distance l through a uniform gas target of number density n. Determination of absolute partial cross sections, without recourse to normalization using the absolute cross section measurements of others, requires mea-

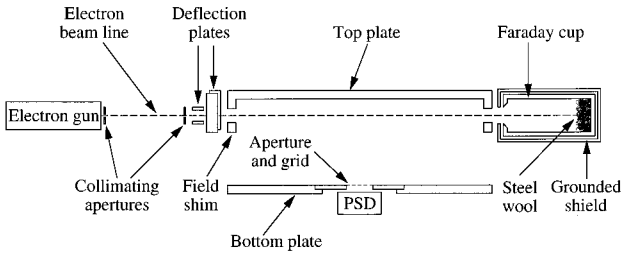

FIG. 1. Schematic diagram of the apparatus.

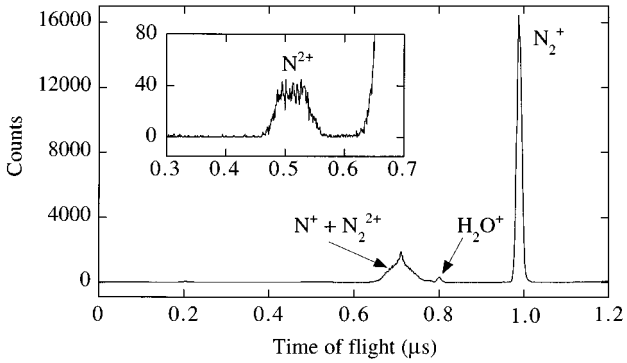

FIG. 2. Time-of-flight spectrum for ions produced by 200-eV electron impact on N_2.

surement of all the quantities on the right-hand side of Eq. (1) and the remainder of this section describes these measurements.

Measurements of N_e and n are relatively straightforward and were described in detail in an earlier paper [4]. Briefly, the electron beam current is collected in the Faraday cup and measured with an electrometer operating in the charge collection mode while the target number density is determined from measurements of the target gas pressure using a capacitance diaphragm gauge.

Measurement of $N_i(X)$ is accomplished with the time-of-flight mass spectrometer. A representative time-of-flight spectrum for N_2 is shown in Fig. 2 which demonstrates that the mass resolution is sufficient to separate product ions having different mass-to-charge ratios. The small contribution to the spectrum due to residual background gas is determined by removing the target gas from the vacuum chamber and again recording the time-of-flight spectrum. The background correction to the measured ion signals is less than 1% except for peaks that overlap with water vapor, the principal background gas present in the vacuum system. For H^+, $N^+ + N_2^{2+}$, and $O^+ + O_2^{2+}$, the peaks that overlap with the ions from water vapor, the background correction is less than 10% except near threshold.

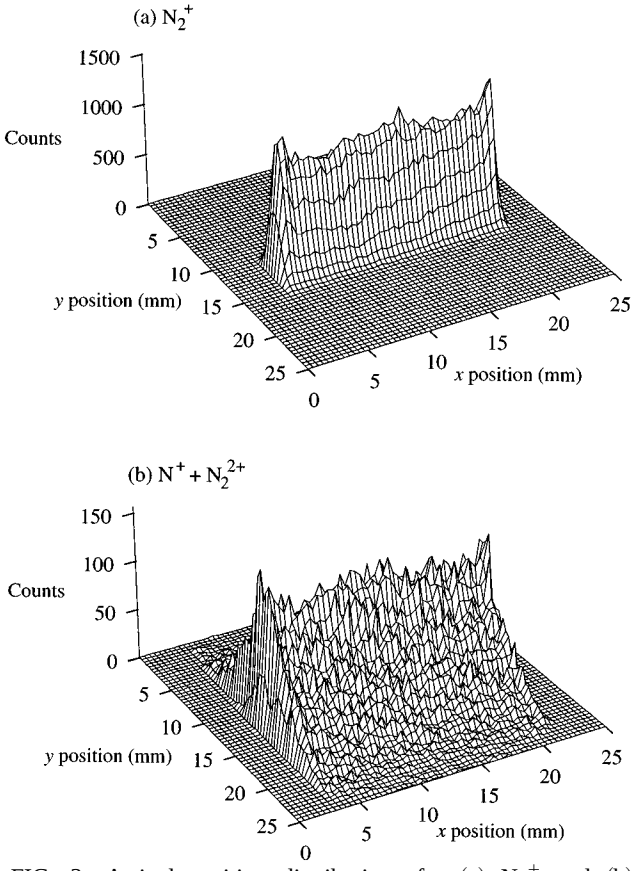

FIG. 3. Arrival position distributions for (a) N_2^+ and (b) $N^+ + N_2^{2+}$ ions produced by 100-eV electron impact. The electron beam is parallel to the x axis.

Figure 3 shows the ion arrival position distribution for both N_2^+ and $N^+ + N_2^{2+}$. The parent ions impact on a narrow strip located immediately beneath the electron beam while energetic fragment ions are detected over a much wider area of the PSD. It is seen, however, that no significant number of

TABLE I. Ion counting statistics and the relative and absolute uncertainties associated with the partial cross sections for H_2, N_2, and O_2. The ion counting statistics represent one standard deviation. The uncertainties for σ (total) come from an appropriately weighted sum of the uncertainties for the partial cross sections.

Target	Cross section	Ion counting statistics (%)	Relative uncertainty (%)	Absolute uncertainty at 200 eV (%)	Absolute uncertainty at all other energies (%)
H_2	$\sigma(H_2^+)$	0.5	±2.0	±3.0	±3.5
	$\sigma(H^+)$	2.0	±3.0	±3.5	±4.5
	σ(total)		±2.0	±3.0	±3.5
N_2	$\sigma(N_2^+)$	0.5	±2.0	±3.0	±3.5
	$\sigma(N^+ + N_2^+)$	1.0	±2.5	±3.5	±4.0
	$\sigma(N^{2+})$	3.0	±3.5	±4.0	±5.5
	σ(total)		±2.0	±3.0	±3.5
O_2	$\sigma(O_2^+)$	0.5	±2.0	±3.0	±3.5
	$\sigma(O^+ + O_2^+)$	1.0	±2.5	±3.5	±4.0
	$\sigma(O^{2+})$	3.0	±3.5	±4.0	±5.5
	σ(total)		±2.0	±3.0	±3.5

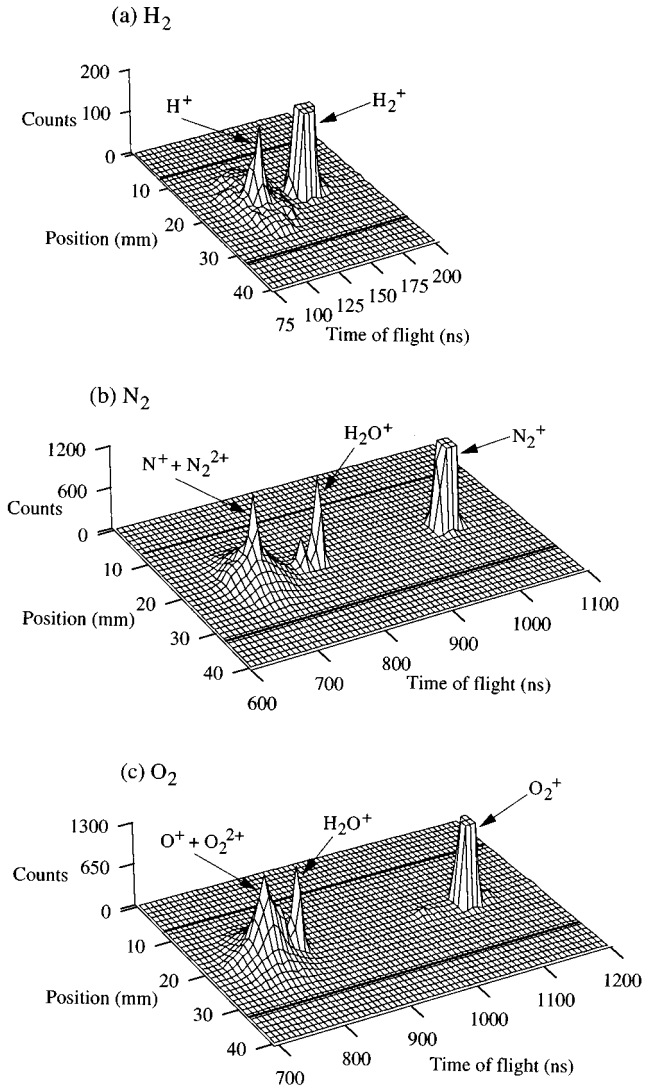

FIG. 4. Position and time-of-flight distributions produced by 1000-eV electron impact on (a) H_2, (b) N_2, and (c) O_2. These data were taken with a 40-mm-diameter PSD and the bold lines at positions of 7.5 and 32.5 mm indicate the boundaries of the 25-mm-diameter PSD.

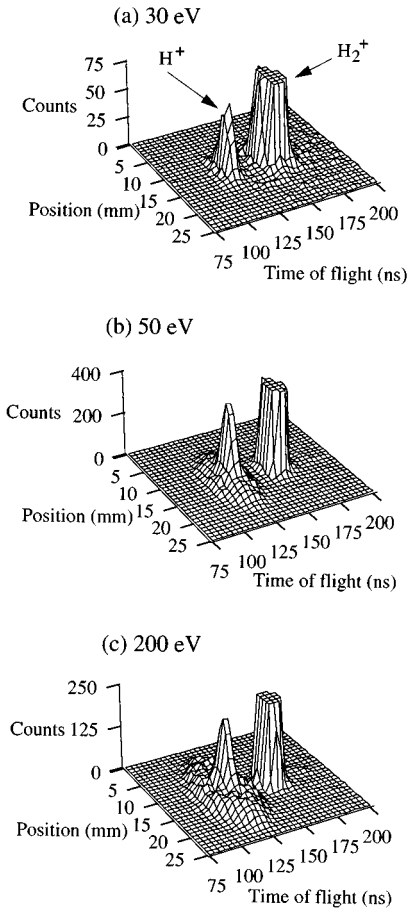

FIG. 5. Position and time-of-flight distributions produced by (a) 30-eV, (b) 50-eV, and (c) 200-eV electron impact on H_2. These data were obtained with a 25-mm-diameter PSD.

ions have sufficient energy to reach the extreme edges of the PSD. For N_2 and O_2, it was determined that all energetic ions from dissociative ionization were collected when the separation between the top and bottom plates was 6.2 cm while for H_2 it was found necessary to reduce this separation to 3 cm in order to collect all of the H^+.

The cross sections for all three target molecules were initially measured using a PSD with a diameter of 25 mm. A few of the more energetic fragment ions, however, impacted near the edges of the PSD and to demonstrate unequivocally that they were indeed being completely collected, the cross sections were remeasured using a larger PSD with a diameter of 40 mm. For these measurements, the dimension of the rectangular aperture, in front of the PSD, was increased to 4.0 cm perpendicular to the electron beam while leaving unchanged the 1.91-cm dimension in the parallel direction. To within the uncertainties stated in Table I, no changes in the measured cross sections were observed, demonstrating that all of the energetic fragment ions were indeed being collected with the 25-mm-diameter PSD. From a knowledge of an ion's flight time and the geometry of the apparatus, the maximum kinetic energy of a fragment ion for which there is complete collection is readily calculated. For the 40-mm-diameter PSD, H^+ ions with kinetic energies up to 17 eV, N^+ and O^+ ions with kinetic energies up to 21 eV, N^{2+} ions with kinetic energies up to 35 eV, and O^{2+} ions with kinetic energies up to 33 eV are completely collected.

An alternative way of presenting the data is illustrated in Fig. 4 in which the ion arrival position distributions of the type shown in Fig. 3 are integrated along the electron beam axis (the x direction in Fig. 3) and combined with the time-of-flight spectrum. The data shown in Fig. 4 were obtained with the 40-mm-diameter PSD and it is evident that all ions are collected for both the 25-mm-diameter and 40-mm-diameter PSD. The width in both position and time of the singly ionized parent molecule peak is due to the spatial extent of the electron beam while the greater width for the fragment ion peaks is due primarily to their initial velocities perpendicular to the electron beam. Figure 5 shows similar plots obtained for H_2 at three additional electron energies. These plots show that there is always a low-energy contribution to the H^+ energy distribution together with a high-energy contribution that grows with increasing electron energy.

Accurate measurement of $N_i(X)$ requires that the detec-

TABLE II. Results for the partial cross sections of H_2.

Energy (eV)	$\sigma(H_2^+)$ (10^{-17} cm^2)	$\sigma(H^+)$ (10^{-18} cm^2)
17	0.611	
20	2.79	
25	5.13	0.455
30	6.90	0.919
35	7.95	1.88
40	8.68	3.07
45	8.96	4.36
50	9.16	5.14
55	9.30	6.08
60	9.37	6.64
65	9.34	7.24
70	9.31	7.48
75	9.22	7.81
80	9.13	7.82
85	9.02	7.94
90	8.90	7.97
95	8.81	8.03
100	8.68	8.00
110	8.39	7.84
120	8.20	7.61
140	7.74	7.04
160	7.32	6.68
180	6.84	6.18
200	6.48	5.69
225	6.09	5.26
250	5.72	4.67
275	5.34	4.28
300	5.07	4.06
350	4.58	3.50
400	4.19	3.03
450	3.83	2.67
500	3.58	2.48
550	3.26	2.17
600	3.05	2.01
650	2.90	1.85
700	2.72	1.75
750	2.61	1.62
800	2.47	1.52
850	2.38	1.40
900	2.26	1.37
950	2.13	1.27
1000	2.02	1.19

TABLE III. Results for the partial cross sections of N_2.

Energy (eV)	$\sigma(N_2^+)$ (10^{-16} cm^2)	$\sigma(N^+ + N_2^{2+})$ (10^{-17} cm^2)	$\sigma(N^{2+})$ (10^{-18} cm^2)
17	0.0242		
20	0.218		
25	0.571		
30	0.998	0.349	
35	1.24	0.969	
40	1.47	1.78	
45	1.63	2.62	
50	1.70	3.40	
55	1.77	4.15	
60	1.83	4.66	
65	1.85	5.11	
70	1.88	5.54	0.0181
75	1.90	5.94	0.0697
80	1.92	6.21	0.129
85	1.92	6.39	0.215
90	1.94	6.67	0.346
95	1.95	6.81	0.463
100	1.94	6.92	0.522
110	1.93	6.95	0.763
120	1.91	6.95	0.974
140	1.87	6.84	1.28
160	1.80	6.62	1.44
180	1.75	6.22	1.61
200	1.68	5.90	1.60
225	1.61	5.37	1.60
250	1.53	5.12	1.48
275	1.47	4.75	1.47
300	1.41	4.53	1.32
350	1.32	4.06	1.21
400	1.24	3.62	1.06
450	1.15	3.34	0.967
500	1.08	3.07	0.830
550	1.02	2.81	0.816
600	0.966	2.54	0.778
650	0.900	2.39	0.717
700	0.862	2.21	0.663
750	0.812	2.09	0.599
800	0.780	2.03	0.605
850	0.752	1.95	0.552
900	0.731	1.86	0.531
950	0.709	1.79	0.514
1000	0.686	1.69	0.492

tion efficiency for each ion species be known. This was determined by repetitively directing an ion beam of appropriate species and energy alternately onto the PSD and into a second Faraday cup (not shown in Fig. 1). For an impact energy of 4.6 keV for singly charged ions, which is the same impact energy employed during cross-section measurements, the detection efficiency was found to have values between 40.0% and 40.5% for all ion species. This same detection efficiency range was observed previously [4] for argon ions using the same grid and PSD and results from a PSD efficiency of 62% and a grid transparency of 65%. The fact that all ions, regardless of their mass-to-charge ratios, are detected with the same efficiency supports the view that, in the present experiment where the ion impact energy on the PSD is large, every ion entering a channel opening of the first microchannel plate of the PSD is detected.

Determination of l, the effective path length along the electron beam from which the collected ions originate, was discussed previously [4] for argon ions. It was shown that the high degree of uniformity of the extraction field coupled with the fact that all argon ions were formed with thermal energy ensured that ions impacting the PSD had originated from a

TABLE IV. Results for the partial cross sections of O_2.

Energy (eV)	$\sigma(O_2^+)$ (10^{-16} cm^2)	$\sigma(O^+ + O_2^{2+})$ (10^{-17} cm^2)	$\sigma(O^{2+})$ (10^{-18} cm^2)
13	0.0127		
15.5	0.0792		
18	0.178		
23	0.395	0.180	
28	0.606	0.840	
33	0.813	1.82	
38	0.994	2.76	
43	1.16	3.56	
48	1.27	4.47	
53	1.37	5.22	
58	1.45	5.88	
63	1.51	6.59	
68	1.56	7.21	
73	1.59	7.60	0.125
78	1.60	7.95	0.200
83	1.62	8.47	0.254
88	1.64	8.73	0.372
93	1.64	9.03	0.462
98	1.64	9.18	0.644
108	1.62	9.47	0.850
118	1.61	9.57	1.01
138	1.57	9.57	1.44
158	1.54	9.47	1.88
178	1.49	9.31	2.09
198	1.45	9.01	2.20
223	1.39	8.64	2.39
248	1.36	8.25	2.35
273	1.28	7.83	2.21
298	1.24	7.46	2.14
348	1.16	6.81	1.96
398	1.08	6.30	1.76
448	1.01	5.78	1.58
498	0.948	5.41	1.40
548	0.904	4.99	1.26
598	0.847	4.68	1.13
648	0.818	4.42	1.10
698	0.777	4.24	1.01
748	0.735	3.96	0.996
798	0.700	3.76	0.853
848	0.684	3.62	0.813
898	0.654	3.42	0.783
948	0.627	3.31	0.752
998	0.607	3.22	0.755

region, directly above the aperture in the bottom plate, whose effective length was equal to the 1.91-cm length of the aperture. In the present measurements, fragment ions resulting from dissociative ionization may have energies of several electron volts and consequently some ions created in the region directly above the aperture with velocities parallel to the electron-beam axis will escape detection. For example, a 15-eV H^+ ion having all of its initial velocity parallel to the electron-beam axis will travel 1.4 cm parallel to the electron-beam axis before reaching the bottom plate. However, the

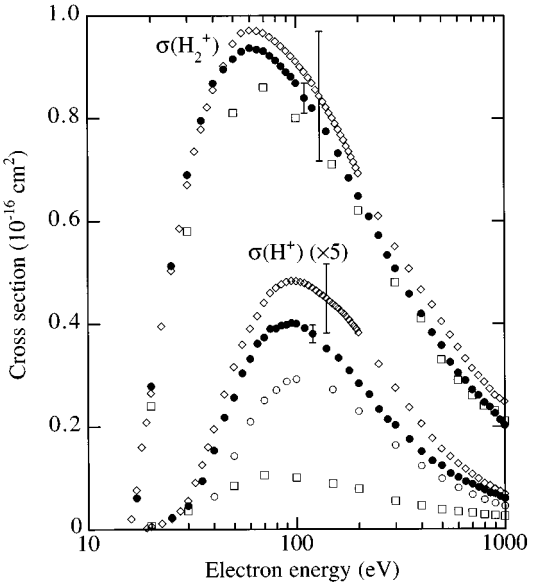

FIG. 6. Present H_2 partial cross sections (●) together with the results of Krishnakumar and Srivastava [12] (◇), Adamczyk *et al.* [17] (□), and Rapp, Englander-Golden, and Briglia [18] (○). The data of Rapp, Englander-Golden, and Briglia are for the production of H^+ with kinetic energies greater than 2.5 eV. Representative error bars are shown for the present work and for the results of Krishnakumar and Srivastava.

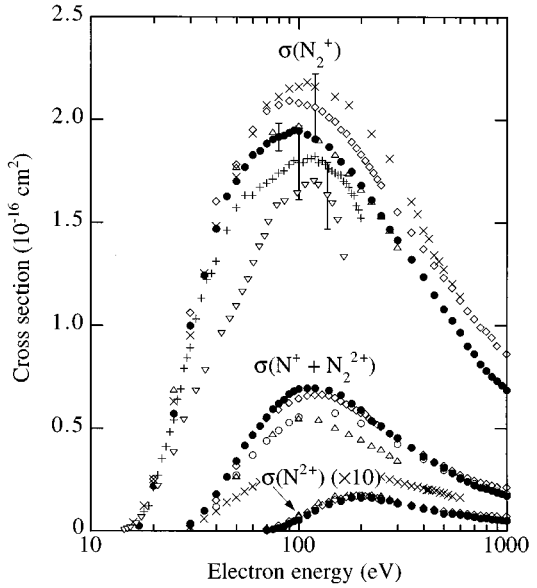

FIG. 7. Present N_2 partial cross sections (●) together with the results of Freund, Wetzel, and Shul [3] (+), Krishnakumar and Srivastava [10] (◇), Märk [14] (▽), Crowe and McConkey [15] (△), Halas and Adamczyk [16] (×), and Rapp, Englander-Golden, and Briglia [18] (○). The data of Rapp, Englander-Golden, and Briglia are for the production of ions with kinetic energies greater than 0.25 eV. Representative error bars are shown for the present work and for the results of Freund, Wetzel, and Shul, of Krishnakumar and Srivastava, and of Märk.

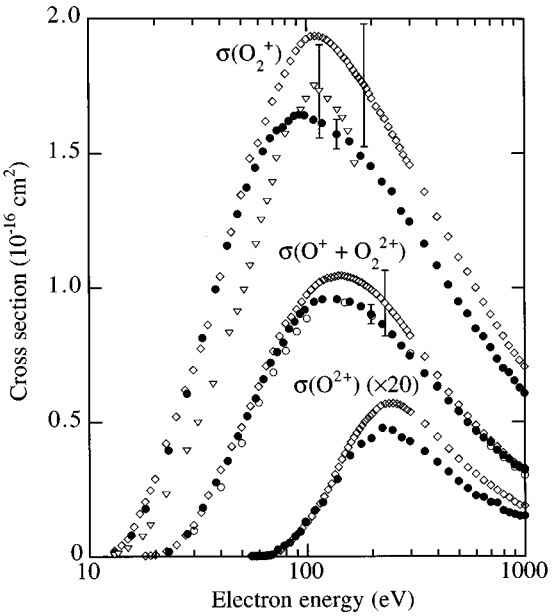

FIG. 8. Present O_2 partial cross sections (●) together with the results of Krishnakumar and Srivastava [11] (◇), Märk [14] (▽), and Rapp, Englander-Golden, and Briglia [18] (○). The data of Rapp, Englander-Golden, and Briglia are for the production of ions with kinetic energies greater than 0.25 eV. Representative error bars are shown for the present work and for the results of Krishnakumar and Srivastava and of Märk.

translational symmetry of the apparatus along the electron-beam axis and the uniformity of the extraction field ensures that for every ion produced in the region directly above the PSD that escapes detection, one from outside this region will be detected. In the case of 15-eV H^+, ions that impact the PSD actually come from a region that is 4.7 cm long although the effective length from which they originate is still given by the 1.91-cm length of the aperture in front of the PSD. Since the top and bottom plates are 19 cm long in the direction parallel to the electron-beam axis, all detected ions originate in a region far removed from the outer edges of the electrodes and thus in a region where the electric field is highly uniform.

III. CROSS-SECTION MEASUREMENTS

Measurement of all the quantities on the right-hand side of Eq. (1), as described in the preceding section, allows direct determination of absolute partial cross sections. Since measurements of n are extremely time consuming, absolute measurements of the cross section for single ionization of the parent molecule were made only at a limited number of electron energies. The absolute cross sections so obtained were then used to place the remaining measurements on an absolute scale. Checks were performed for each target molecule to establish the independence of the measured cross sections with respect to both the target gas pressure and electron beam current.

A detailed analysis of the experimental uncertainties has been given previously [4]. Table I gives the ion counting statistics and the relative and absolute uncertainties for all cross sections measured in this work. The relative uncertainties come from the ion counting statistics and a ±0.5% uncertainty in the electron beam current measurement. The absolute uncertainties in the cross sections come from the ion counting statistics, a ±0.5% uncertainty associated with determination of the detection efficiency, a ±0.5% uncertainty in the electron beam current measurement, a ±0.5% uncertainty in the calibration of the electrometer used for the electron beam current measurement and PSD detection efficiency determination, a ±1% uncertainty in the target length, a ±2.5% statistical uncertainty and a ±1% calibration uncertainty in the pressure measurement with the capacitance diaphragm gauge, and a ±0.2% uncertainty in the temperature measurement needed for calculation of the number density. The energy of the electron beam was established to better than ±1 eV by observing the threshold for He^+ formation.

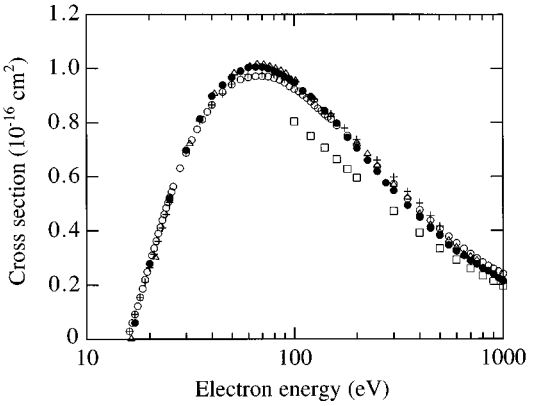

FIG. 9. Present H_2 total cross section (●) together with the results of Rapp and Englander-Golden [1] (○), Cowling and Fletcher [8] (+), Schram *et al.* [6,7] (□), and Tate and Smith [5] (△).

IV. RESULTS AND DISCUSSION

The measured partial cross sections for H_2, N_2, and O_2 are listed in Tables II–IV and are plotted in Figs. 6–8 together with previously published partial cross sections. Total cross sections obtained as the sum of the present partial cross sections (i.e., the counting cross section) are shown in Figs. 9–11 together with previously published direct measurements of the absolute total cross sections. The total cross sections of Tate and Smith [5], Rapp and Englander-Golden [1], Schram *et al.* [6,7], Cowling and Fletcher [8], and Asundi, Craggs, and Kurepa [9] were obtained from measurements of total charge production (i.e., the gross ionization cross section). Their cross sections are thus the sum of the partial cross sections weighted by the charge of the ion. In the case of H_2 these two types of total cross section are identical since all ions are singly charged while for N_2 and O_2, where multiply charged ions occur, the difference between the two types of total cross sections is estimated to be less than 2%. The total cross section data for H_2 show excellent agreement except for the measurements of Schram *et al.* [6,7], which lie lower than all other results. The total cross sections for N_2 and O_2 also show agreement within the combined uncertainties of the measurements except for the results of both Tate and Smith [5] and Asundi, Kurepa, and Craggs [9], which probably lie higher than all other results due to their use of McLeod gauges uncorrected for the mer-

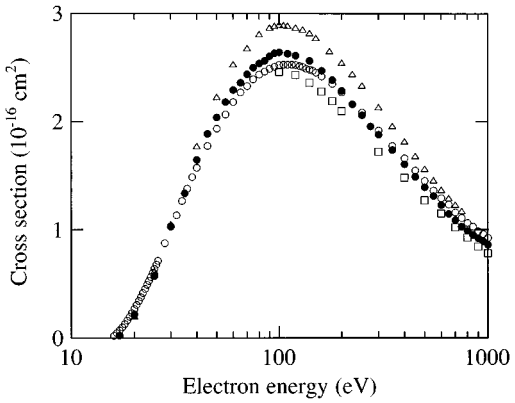

FIG. 10. Present N_2 total cross section (●) together with the results of Rapp and Englander-Golden [1] (○), Schram *et al.* [6,7] (□), and Tate and Smith [5] (△).

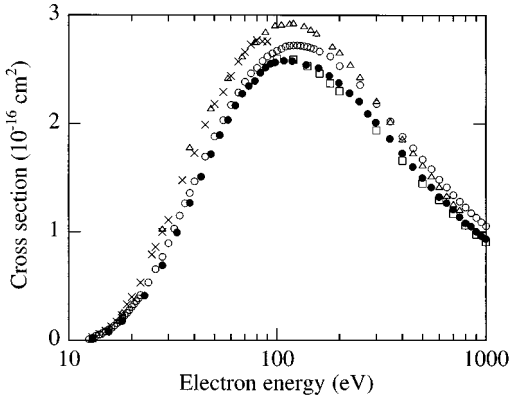

FIG. 11. Present O_2 total cross section (●) together with the results of Rapp and Englander-Golden [1] (○), Schram *et al.* [6,7] (□), Tate and Smith [5] (△), and Asundi, Craggs, and Kurepa [9] (×).

cury pumping effect. For all three targets, the absolute values of Rapp and Englander-Golden [1] agree with the present measurements to within the combined uncertainties.

Previously published partial cross sections are shown in Figs. 6–8 with the exception of those of Peterson [2], which are clearly in error. It should be noted that previous partial cross-section measurements generally report uncertainties of ±8% to ±15% while the uncertainties for the present results are ±5.5% or less. The only absolute measurements shown, other than the present results, are the N_2^+ cross sections of Freund, Wetzel, and Shul [3], which agree with the present results to within the combined uncertainties. Krishnakumar and Srivastava [10–12] measured relative cross sections that were then normalized using the He cross section recommended by Bell *et al.* [13], which agrees very well with the He cross section of Rapp and Englander-Golden [1]. All of the cross sections of Krishnakumar and Srivastava [10–12] agree with the present results to within the combined uncertainties, however, Krishnakumar and Srivastava would agree even better with the present results had they directly normalized to Rapp and Englander-Golden's total cross sections for H_2, N_2, and O_2 instead of indirectly normalizing to Bell *et al.*'s He cross section. Märk [14], Crowe and McConkey [15], and Halas and Adamczyk [16] measured relative cross sections, which were then normalized using the total cross sections of Rapp and Englander-Golden [1]. The N_2^+ and O_2^+ cross sections of Märk [14] have an energy dependence that is not consistent with that observed by others. The N_2 results of Crowe and McConkey [15] agree well with the present results while those of Halas and Adamczyk [16] disagree with the present results. The H_2^+ results of Adamczyk *et al.* [17] are lower than the present results due to their normalization to the results of Schram *et al.* [6] while the H^+ cross sections of Adamczyk *et al.* lie much lower than the present results probably due to discrimination of their mass spectrometer against energetic H^+ ions. The data of Rapp, Englander-Golden, and Briglia [18], which are included for completeness, are for the production of H^+ with kinetic energies greater than 2.5 eV in H_2 and for the production of ions with kinetic energies greater than 0.25 eV in N_2 and O_2.

V. CONCLUSION

An apparatus and experimental method are described that permit direct measurements of absolute partial cross sections for electron-impact ionization of molecules. The apparatus is simple in concept and embodies a short path length time-of-flight mass spectrometer and a position-sensitive detector for the product ions. The combination of these two devices makes it possible to unequivocally capture all energetic fragment ions formed in dissociative processes and to detect them with known efficiency. Difficulties that plagued many of the earlier investigations have thereby been eliminated.

ACKNOWLEDGMENTS

We gratefully acknowledge support by the Atmospheric Sciences Section of the National Science Foundation, the National Aeronautics and Space Administration, and the Robert A. Welch Foundation. In addition, we have benefited from useful discussions with Y.-K. Kim and B. Van Zyl.

[1] D. Rapp and P. Englander-Golden, J. Chem. Phys. **43**, 1464 (1965).

[2] J. R. Peterson, in *Proceedings of the Third International Conference on the Physics of Electronic and Atomic Collisions, London, 1963*, edited by M. R. C. McDowell (North-Holland, Amsterdam, 1964), p. 465.

[3] R. S. Freund, R. C. Wetzel, and R. J. Shul, Phys. Rev. A **41**, 5861 (1990).

[4] H. C. Straub, P. Renault, B. G. Lindsay, K. A. Smith, and R. F. Stebbings, Phys. Rev. A **52**, 1115 (1995).

[5] J. T. Tate and P. T. Smith, Phys. Rev. **39**, 270 (1932).

[6] B. L. Schram, F. J. De Heer, M. J. Van der Wiel, and J. Kistemaker, Physica **31**, 94 (1965).

[7] B. L. Schram, H. R. Moustafa, J. Schutten, and F. J. De Heer, Physica **32**, 734 (1966).

[8] I. R. Cowling and J. Fletcher, J. Phys. B **6**, 665 (1973).

[9] R. K. Asundi, J. D. Craggs, and M. V. Kurepa, Proc. Phys. Soc. **82**, 967 (1963).
[10] E. Krishnakumar and S. K. Srivastava, J. Phys. B **23**, 1983 (1990).
[11] E. Krishnakumar and S. K. Srivastava, Int. J. Mass Spectrom. Ion Proc. **113**, 1 (1992).
[12] E. Krishnakumar and S. K. Srivastava, J. Phys. B **27**, L251 (1994).
[13] K. L. Bell, H. B. Gilbody, J. G. Hughes, A. E. Kingston, and F. J. Smith, J. Phys. Chem. Ref. Data **12**, 891 (1983).
[14] T. D. Märk, J. Chem. Phys. **63**, 3731 (1975).
[15] A. Crowe and J. W. McConkey, J. Phys. B **6**, 2108 (1973).
[16] S. Halas and B. Adamczyk, Int. J. Mass Spectrom. Ion Phys. **10**, 157 (1973).
[17] B. Adamczyk, A. J. H. Boerboom, B. L. Schram, and J. Kistemaker, J. Chem. Phys. **44**, 4640 (1966).
[18] D. Rapp, P. Englander-Golden, and D. D. Briglia, J. Chem. Phys. **42**, 4081 (1965).